Estimating Heavy Oil Viscosity from Crosswell Seismic Data

Fereidoon Vasheghani * and L.R. Lines**

Department of Geoscience

University of Calgary

Calgary, Alberta, Canada T2N 1N4

*Now with ConocoPhillips Canada, 401 – 9th Ave SW, Calgary, Alberta, Canada T2P 2H7

** Corresponding author (lrlines@ucalgary.ca)

ABSTRACT

The reliable estimation of oil viscosity is crucial for simulating fluid flow in heavy oil fields. While there are methods for measuring heavy oil viscosity from borehole samples, it would be very useful to reliably estimate fluid viscosity between wells using seismic data. This paper applies a methodology for estimating viscosity from crosswell seismic data, by using seismic traveltime tomography, seismic attenuation tomography and rock physics. Heavy oil sands are viscoelastic and the oil affects the attenuation of seismic waves, which can be measured in terms of the seismic quality factor, Q. We relate seismic Q to fluid viscosity in a two stage process. Q tomograms are estimated from crosswell seismic data by applying a tomographic technique proposed by Quan and Harris (1997). Q is then related to fluid viscosity by utilizing BISQ (Biot Squirt Theory), a poroviscoelastic model that couples the simultaneous Biot and squirt flow mechanisms. The classical BISQ equations of Dvorkin and Nur (1993) are modified to allow for two phase flow of bitumen and water. By applying Q tomography and BISQ, we estimate viscosity tomograms between boreholes. The estimated viscosity tomograms show ambiguity because for every Q value, more than one viscosity value can be calculated. Despite this ambiguity, our technique demonstrates that seismic data have the potential to be used for estimation of fluid viscosity in heavy oil reservoirs, especially if some constraints can be placed on the viscosity values. We apply our methodology to reservoir characterization of the Grand Rapids formation in the Athabasca oil sands. Future applications to time-lapse monitoring of heavy oil reservoirs are recommended.

KEY WORDS: seismic attenuation, Q, viscosity, tomography, heavy oil reservoir characterization.

Introduction

The main property of heavy oils is that such fluids are practically immobile at the original reservoir condition and therefore, more energy is required to produce such oils than in the production of conventional oil reservoirs. Viscosity is a measure of fluid's resistance to flow. The higher the viscosity, the more energy is required to move the fluid. In order to make the production of heavy oils possible, the viscosity has to be lowered. This is usually done by heating the oil in-situ. Viscosity of the heavy oil decreases as the temperature increases. The amount of heat required to mobilize the oil to a degree that it is commercially recoverable depends on the original viscosity of the oil at reservoir conditions. The performance of such production scenarios depends on the understanding of the variation of the heavy oil viscosity within the reservoir.

Traditionally in seismic rock physics, it is assumed that the shear modulus of the fluids is zero, or that fluids do not support shear. While the assumption of zero or negligible fluid shear modulus may be acceptable for fluids with lower viscosities such as conventional oils or water, it is generally not an appropriate approach assumption in the case of heavy oils.

Viscoelastic seismic response

The wave equation is a partial differential equation that describes the propagation of waves in a material in terms of particle displacement. In order to derive the wave

equation, two constitutive equations are required: an equation of motion, and a stress-strain relationship.

Viscoelastic behavior is a time dependent, mechanical non-instantaneous response of a material body to variations of applied stress (Carcione, 2007). This means the response of the medium to stress is not immediate. The delay is due to the viscous behavior of the material. The wave equation can be adjusted to represent a viscoelastic wave equation by using the appropriate stress-strain relationship.

A reservoir rock is generally formed of a porous frame as the host with fluids in the pore space. Laboratory measurements show that heavy oils are viscoelastic materials (Eastwood, 1993; Han et al., 2007) that have non-negligible shear moduli, and support shear wave propagation (Das and Batzle, 2008). When a rock is saturated with heavy oils, its behavior consequently becomes viscoelastic (Behura et al., 2007).

Biot (1962) explained the theory of propagation of stress waves in the medium for an elastic porous frame filled with viscous fluid. In his theory, the solid part is assumed to behave perfectly elastically. In a perfectly elastic medium, the loss of energy due to friction does not occur; therefore, in Biot's theory, the losses caused by a solid frame are ignored (Wyllie et al., 1962). Another assumption is that the fluid is compressible and can flow relative to the solid frame. In Biot's model, the fluid is forced to participate in an oscillatory motion by viscous forces and inertial coupling (Dvorkin and Nur, 1993). This motion will cause friction and hence the energy will be lost in the form of heat.

When pressure is applied to a porous material saturated with fluids, pores with lower aspect ratios (penny shaped pores) undergo a bigger change in volume; consequently the fluid inside such cracks has to flow toward the pores with higher aspect

ratio. This phenomenon is known as “squirt flow”. Such flow will affect the viscoelastic behavior of the saturated rock. These modes of solid-fluid interaction (Biot, and squirt flow effects) are interconnected and simultaneously influence each other as well as the process of seismic wave propagation. This was shown by Dvorkin and Nur (1993) who developed an integrated Biot plus squirt flow theory known as BISQ. In this theory both mechanisms are simultaneously considered and the behavior of rocks is related to measurable and macroscopic reservoir and fluid properties such as oil viscosity, and reservoir permeability.

Seismic attributes and viscosity

The amplitude of a wave is directly related to its energy. In a viscoelastic medium, the seismic wave amplitude decreases with propagation distance. Such reduction in the amplitude is on top of all other forms of energy loss (such as geometric spreading or scattering), and as mentioned earlier, this attenuation of amplitude (or energy) is due to friction. The quality factor, which is inversely proportional to the attenuation, is defined as the ratio of energy over the loss of energy per cycle multiplied by 2π (Aki and Richards, 2002).

$$Q = \frac{2\pi E}{\Delta E} \tag{1}$$

This definition implies that attenuation of the energy is frequency dependant. In order to travel from one location to another, the waves with higher frequencies (lower wavelengths) go through more cycles and hence get attenuated faster. At seismic frequency ranges, the quality factor is related to the reservoir parameters through the following BISQ equations as derived by Dvorkin and Nur (1993):

$$V_p = \frac{1}{\mathrm{Re}\left(\sqrt{Y}\right)}, \tag{2}$$

$$Q = \frac{\mathrm{Re}\left(\sqrt{Y}\right)}{2\,\mathrm{Im}\left(\sqrt{Y}\right)}, \tag{3}$$

Where in the above

$$Y = \frac{(1-\varphi)\rho_m + \varphi\rho_f}{K_{fr} + \frac{4}{3}\mu_{fr} + F_{sq}\frac{\alpha^2}{\varphi}} \tag{4}$$

$$F_{sq} = F\left[1 - \frac{2J_1(\xi)}{\xi J_0(\xi)}\right] \tag{5}$$

$$\xi = \sqrt{\frac{i\omega R^2 \eta_f \varphi}{kF}} \tag{6}$$

$$\alpha = 1 - \frac{K_{fr}}{K_m} \tag{7}$$

$$F = \frac{1}{\varphi}\left(\frac{\varphi}{K_f} + \frac{1-\varphi}{K_m} - \frac{K_{fr}}{K_m{}^2}\right) \tag{8}$$

In the above equations η_f is fluid viscosity, k is permeability, φ is porosity and ρ_f and ρ_m are fluid and solid densities, respectively, K_m, K_f and K_{fr} are the solid, fluid and the frame bulk moduli, respectively. μ_{fr} is the frame shear modulus, J_n is Bessel function of

order n, ω is angular frequency, and *R* is the characteristic squirt flow length. Variation of the quality factor with viscosity for the reservoir properties, summarized in Table 1, is shown in Figure 1.

The experiment (Behura et al., 2007) shows that the variation of the quality factor with temperature exhibits the same trend (i.e. in either direction, it decreases to a minimum and then increases). The experiments which show a "hockey stick" shape to the Q versus viscosity plot are in agreement with the computational models, as shown in the Zener models of Carcione (2007) and in Vasheghani and Lines (2009).

Methodology: The workflow for estimating viscosity from crosswell seismic data

The BISQ equations establish the relation between quality factor and fluid viscosity. Therefore, the first step in the quest for viscosity is to estimate *Q* from seismic data. Crosswell seismic data are most desirable for this type of analysis than surface seismic recordings for several reasons. The crosswell energy does not travel through the near surface layer, which is highly absorptive and reduces the quality of the signal. Also, in crosswell seismology, the survey is done right at the zone of interest and this reduces some of the uncertainties in the processing and interpretation of the results. Finally, crosswell data are usually run at higher frequencies than surface seismic surveys. This means that with any given quality factor, crosswell seismic energy is attenuated more than its surface seismic counterparts, which in turn means that it is easier to measure attenuation and the results are less sensitive to the errors. The workflow for estimating fluid viscosity from crosswell seismic data is shown in Figure 2.

Tomography

Tomography is an imaging technique that uses the information carried by penetrating waves, and has applications in many areas such as radiology, geophysics and materials science. Seismic tomography is a method for estimating the earth's properties such as P-wave velocity (using travel time tomography) or quality factor (using attenuation tomography). Such methods are formulated as an inverse problem in which the properties of the model will be estimated from the measured response of the model.

In travel time tomography, the wave velocity in the material between the two wells is estimated from the arrival times of the waves travelling between the source in one well and the receivers in the other well. In attenuation tomography, the attenuation coefficient of the material is calculated using the changes in the frequency content of the signal. Remember that a signal is composed of a range of frequencies, and as mentioned earlier, the high frequency components of the signal are attenuated faster. This means that the frequency distribution of the wave changes between the source and receiver, and such variation is converted into the attenuation coefficient, which in turn can be converted to quality factor.

One application of seismic tomography is in crosswell seismic imaging where rays travel from sources in one well to receivers in a nearby well. The traveltime tomography for such data has been described by McMechan (1983) and by Lines (1991), among others, and basically involves the solution of traveltime equations of the form:

$$t_i = \sum_j \ell_{ij} s_j . \qquad (9)$$

Here t_i is the traveltime for the ith ray, ℓ_{ij} is the distance of the ith ray in the jth cell and s_j is the slowness (reciprocal velocity) of the jth cell. While many of the original traveltime tomography applications used square pixels as cells, as in Lines (1991), we use a more parsimonius parameterization of the subsurface in an algorithm due to Washbourne et al. (2002). The algorithm of Washbourne et al. uses velocity cells that are a set of layers described by Chebyshev polynomials. Traveltime tomography establishes the ray paths for crosswell direct arrivals and subsequently solves for velocity estimates in the region between boreholes by iteratively solving for the velocities in the cells. Once the traveltime tomography has been completed, the ray paths can be used in solving the attenuation tomography equations. Also, the velocity cells from the Washbourne algorithm can be pixilated for use in attenuation tomography.

Attenuation tomography is the second step in this process and for these purposes we use the algorithm proposed by Quan and Harris (1997). As the rays travel in each cell, there is attenuation of wave amplitudes and a lowering of the frequency content as the waves propagate from source to receiver. The degree of the frequency lowering can measured and related to the attenuation. The change in the frequency content of the signal is quantified by the change in its centroid frequency, where the centroid frequency for a signal's amplitude spectrum is defined as:

$$\bar{f} = \frac{\int_0^\infty fS(f)df}{\int_0^\infty S(f)df} \quad . \tag{10}$$

Variation of the centroid frequency for a signal travelling from source to receiver is related to the attenuation coefficient of all cells using the following tomographic equation from Quan and Harris (1997):

$$\sum_j \ell_{ij} \alpha_{0,j} = \frac{f_s - f_R}{\sigma_s^2} \tag{11}$$

where subscripts i and j denote the ray cell numbers respectively, $\alpha_{0,j}$ is attenuation coefficient in the jth cell, f_s and f_R are the centroid frequencies at the source and receiver locations, respectively, and σ_s^2 is the variance of the source signal spectrum. For computational convenience, Quan and Harris (1997) define their attenuation, $\alpha_{0,}$ to be related to the usual attenuation coefficient, α, by the linear relationship, $\alpha = \alpha_{0,} f$.

The values of the velocities from traveltime tomography and the values of the attenuation coefficients from attenuation tomography can be combined to produce a *Q* tomogram by the following relationship.

$$Q = \frac{\pi}{\alpha \lambda} = \frac{\pi}{\alpha_0 V} \tag{12}$$

where λ is wavelength.

The *Q* tomogram is then used as input for the viscosity computations. Once the quality factor values are estimated, viscosity values can be estimated through the BISQ equations described earlier; however, such equations require that the remaining reservoir parameters such as porosity, permeability, fluid and solid elastic moduli, as listed in Table 1, be known in advance. Such reservoir parameters are usually known through well data and other sources of information,

Alberta heavy oil crosswell case study

The Athabasca oil sands in the province of Alberta, Canada, are considered to be the largest deposits of bitumen in the world and are estimated to be 1.7 to 2.5 trillion barrels, out of which 170 to 300 billion barrels are economically recoverable with present enhanced oil recovery technology. The bitumen reserves contain oils with gravities ranging from 8 to 12° API, and viscosities ranging up to several million centipoise, which are hosted in the reservoirs of varying age, ranging from Devonian to early Cretaceous. The heavy oil reservoir of this study is located in the Grand Rapids formation in the western Athabasca area and is within a sequence of Quaternary, Cretaceous and Devonian sediments on the Precambrian crystalline basement. Figure 3 gives the location of the crosswell survey. Cretaceous units include the shales and sands of the Labiche, Viking and Joli Fou formations of the Colorado Group and Grand Rapids, Clearwater and McMurray formations of the Mannville Group. The Grand Rapids formation is divided into three main subunits of the upper, middle and lower Grand Rapids. These subunits are separated by shale and silt intervals. The uppermost unit, called the Upper Grand Rapids, is mainly formed of fine to medium grained sand and is bitumen saturated. This subunit forms the zone of interest. The Joli Fou shale which overlies the upper Grand Rapids, acts as the cap rock to the reservoir.

Two vertical wells are used as the source and receiver wells in the crosswell data acquisition. The separation between the source and receiver wells at the surface is 140 meters and the zone of interest is located at the depth interval of 188 m to 218 m.

Clamped vibrator type sources and single clamped geophones are used in the survey. The source and receiver spacing is 1.5 meters in both wells, which provides a finely sampled dataset. The crosswell survey geometry is outlined in Figure 4. The diagram shows that the shallow recorders (63 receivers from depth of 8.5 m to 101.5 m) have only recorded the signal from deeper sources, while the deeper recorders (108 receivers from depth of 103 m to 263.5 m) have recorded the signal from the entire source array. A total of 171 receiver gathers have been recorded. The frequency content of the data generated by the vibratory source ranges from 30 Hz to 600 Hz with the dominant frequency of 420 Hz. This is much higher than the typical surface seismic dominant frequency. The sampling interval is 0.5 ms (sampling frequency of 2000 Hz) which allows the Nyquist frequency of 1000 Hz.

The density of the direct arrival rays, calculated using straight rays, is shown in Figure 5. The scale represents the total length of rays per unit cross sectional area. Figure 6 shows a common receiver gather from a receiver at the depth of 205 m. Travel times can be obtained by locating the arrivals and will be used in travel time tomography. Once the travel times are known, the signal can be isolated in a trace by using a window of a specific length. The frequency content of the signal is then obtained through Fourier transform, and the centroid frequency is calculated from the resulting amplitude spectrum.

Data from 15 other wells around the crosswell profile are used for the geostatistical construction of the reservoir data (Figure 7).

The profile between the source and receiver wells is divided into 1 m thick layers in order to perform the travel time tomography using the Chebyshev polynomials

technique. The resulting velocity tomogram is shown in Figure 8. The well logs on the sides of the tomogram show the velocity calculated from the sonic log and the velocity estimated from crosswell tomography. The velocity dispersion observed at the well bore results from the difference between sonic and crosswell seismic frequencies.

Within the zone of interest, which is saturated with bitumen and water, the sonic velocity is greater than the crosswell seismic velocity. This is in agreement with previous observations (Schmitt, 1999). This phenomenon is called the velocity dispersion, and the medium is called dispersive.

In order to complete the attenuation tomography, each layer defined in the travel time tomography, is divided into 140 cells, 1 m by 1 m in size each. The tomography is then carried out using the pixilated tomography technique. The output is an attenuation coefficient tomogram shown in Figure 9.

Knowing the velocity for each grid cell from the travel time tomography, the attenuation coefficient is converted to the quality factor Q (Figure 10) using the equation (12).

The interval above the reservoir (178 m – 188 m) corresponds to the Joli Fou shale, which acts as the cap rock to the reservoir. This interval is easily identified in the quality factor tomogram while it is hardly identifiable on the velocity tomogram. This is due to the fact that the shale is saturated with water and does not contain viscous material and therefore does not attenuate the energy as much as the other zones. The distinct red zone near the top of the tomogram (depth interval 178 m – 188 m) corresponds to the cap rock shale.

Estimating reservoir properties

Porosity, permeability and water saturation of the rock are measured in the lab from the core samples. This allows the direct geostatistical estimation of the porosity and permeability for the entire crosswell area. Sequential Gaussian simulation technique is used to generate 10 different realizations for porosity and permeability. The averages of these realizations are used as the estimates of porosity and permeability of the reservoir. After some algebraic operations, it is proven that quality factor is not a function of density. This means that prior knowledge of solid and fluid densities in not necessary. Direct measurements of the elastic properties of the material such as bulk and shear moduli are not available at the wellbores; therefore these parameters are calculated using the Hashin-Shtrikman relations. Hashin-Shtrikman relations take the volume fraction of the various constituents of the reservoir rock, together with their elastic properties, and calculate the elastic properties of the saturated rock. In the current case, it is assumed the rock is formed of solid frame filled with connate water and bitumen. It is also assumed that the solid frame is composed of quartz and clay minerals. Therefore, the constituents of the saturated rock are quartz, clay, water and bitumen.

Knowledge of the volume fractions of the shale and water, as well as already known porosity values is sufficient for calculating the volume fraction of the other constituents (quartz and bitumen), because of the following constraints:

$$S_o + S_w = 1 \tag{13}$$

$$V_{ss} + V_{sh} = 1 \quad . \tag{14}$$

The volume fraction of shale (clay minerals) at each well location can be derived from the gamma ray log through the following familiar equation:

$$V_{sh} = \frac{GR_{\log} - GR_{\min}}{GR_{\max} - GR_{\min}}. \qquad (15)$$

Water saturation measurements from core samples are also available at 8 wells. Sequential Gaussian simulation technique is used to generate 10 different realizations for shale volume and water saturation. The averages of these realizations are used as the final estimates. The volume fractions of sand and bitumen are calculated from equations (13) and (14).

As for the elastic properties of each constituent (quartz, clay, water and bitumen) and the characteristic squirt flow length, the values given in Table 2 are assumed. The generalized form of the Hashin-Shtikman equations which can be applied to more than two phases (Mavko et al, 2003) is used to calculate the elastic properties of the saturated rock.

Viscosity inversion

The final step of the workflow, shown in Figure 2, is to use *Q* values as well as the reservoir parameters, and estimate the viscosity of the heavy oil in the zone of interest. The nature of *Q*-viscosity relation implies that for every *Q*, two viscosity values can be predicted, consequently, the resulting viscosity tomogram is non unique and ambiguous.

The viscosity tomograms, generated using the left and right slopes of the $Q-\eta_f$ curves, are shown in Figures 11 and 12, respectively. The top 5 meters of the reservoir is not shown in the tomograms because it corresponds to the top water zone where the water saturation is greater than 80%. Measured viscosity values at the well locations are not available; therefore it is not possible to validate the final viscosity estimates. Although lack of real measurements of the viscosity prevents the validation of the final results, these tomograms demonstrate that seismic data have the potential to be used for heavy oil viscosity characterization. Based on our knowledge on what is known about heavy oil viscosities in the Grand Rapids Formation, it is believed that Figure 12 gives a more probable viscosity tomogram than Figure 11.

Conclusions

Contrary to the conventional seismic approach in which it is assumed that fluids do not support shear, when dealing with the Athabasca heavy oils, the shear properties of the fluids should not be ignored. Heavy oils are viscoelastic materials and will cause the porous material to act viscoelastically. The effects of shear properties of heavy oils are reflected in the attenuation of seismic waves; therefore, the seismic response is sensitive to the shear character of heavy oils.

The quality factor, which is inversely proportional to attenuation, can be related to the oil viscosity through the BISQ equations. This means that when a *Q* tomogram is generated, it can be converted to the fluid viscosity tomogram. However, the resulting viscosity tomogram is ambiguous because for every given quality factor, there is more than one value for viscosity. These viscosity values are a few orders of magnitude apart;

thus, previous knowledge of the fluid properties in the region can help identify the more realistic viscosity tomogram.

In this study we have developed a methodology for estimating viscosity tomograms for heavy oil sands using crosswell data. A very valuable application would be to repeat the crosswell experiment after some period of steam injection and to compute another set of viscosity tomogram. This time-lapse application of viscosity tomography and the interpretation of the largest changes in viscosity should allow us to image the steamed zones where viscosity is lowered. Hence this time-lapse view of viscosity change should prove to be a useful tool in the enhanced recovery of heavy oil.

Acknowledgements

The authors wish to thank the sponsors of the Consortium for Heavy Oil Research by University Scientists (CHORUS), the Alberta Ingenuity Centre for In-situ Energy (AICISE), and the Natural Sciences and Engineering Research Council of Canada (NSERC) for financial support of this research. We thank Schlumberger, and especially Dr. Bob Godfrey and Dr. Tom Morgan for offering technical assistance and providing full access to their resources during this research. We especially thank Laricina Energy for providing the crosswell seismic data used in this study. Finally, we thank Joan Embleton for arranging the support of this research.

References

Aki, K., and Richards, P.G., 2002. Quantitative Seismology, Second Edition, University Science Books, Sausalito, California.

Behura, J., Batzle, M., R. Hofmann, R. and Dorgan, J., 2007, Heavy oils: Their shear story: Geophysics, **72**, E175-E183.

Biot, M. A., 1962, Mechanics of deformation and acoustic propagation in porous media: Journal of Applied Physics, **33**, 1482-1498.

Carcione, J. M., 2007, Wave Fields in Real Media - Wave Propagation in Anisotropic, Anelastic, Porous and Electromagnetic Media: Elsevier, Amsterdam, The Netherlands.

Das, A., and Batzle, M., 2008, Modeling studies of heavy oil in between solid and fluid properties: The Leading Edge, **27**, 1116-1123.

Dvorkin, J., and Nur, A., 1993, Dynamic poroelasticity: a unified model with the squirt flow and the Biot mechanism: Geophysics, **58**, 524-533.

Dvorkin, J., Nolen-Hoeksema, R., and Nur, A., 1994, The squirt flow mechanism: macroscopic description: Geophysics, **59**, 428-438.

Eastwood, J., 1993, Temperature-dependent propagation of P-waves and S-waves in Cold Lake oil sands: Comparison of theory and experiment: Geophysics, **58**, 863-872.

Gassmann, F., 1951, Über die Elastizität poröser Medien: Vierteljahrsschrift der Naturforschenden Gesselschaft in Zürich, **96**, 1-23.

Han, D., Yao, Q., and Zhao, H.-Z., 2007, Complex properties of heavy oil sand: 77th Annual International Meeting, SEG Expanded Abstracts, **26**, 1609-1613.

Lines, L.R., 1991, Applications of tomography to borehole and reflection seismology: The Leading Edge, **10,** no.7, 11-17.

Mavko, G. M., Mukerji, T., and Dvorkin, J., 2003, The Rock Physics Handbook: Tools for Seismic Analysis in Porous Media: Cambridge University Press.

McMechan, G., 1983, Seismic tomography in boreholes, Geophys. J.R. astr. Soc., 74, 601-612.

Quan, Y., and Harris, J.M., 1997, Seismic attenuation tomography using frequency shift method: Geophysics, **62**, 895-905.

Schmitt, D. R., 1999, Seismic attributes for monitoring of a shallow heated heavy oil reservoir: A case study: Geophysics, **64**, 368-377.

Vasheghani, F., and Lines, L.R., 2009, Viscosity and Q in heavy-oil reservoir characterization: The Leading Edge, **28**, 856-860.

Washbourne, J. K., Rector, J.W., and Bube, K.P., 2002, Crosswell traveltime tomography in three dimensions: Geophysics, **67**, 853-871.

Wyllie, M. R. J., Gardner, G. H.F., and A. R. Gregory, A.R., 1962, Studies of elastic wave attenuation in porous media: Geophysics, **27**, 569-589.

Figure Captions

Figure 1: Variation of quality factor with fluid viscosity predicted by BISQ theory. Reservoir parameters are given in Table 1.

Figure 2: Workflow for estimating viscosity from crosswell seismic data.

Figure 3: Location of the crosswell survey in the Athabasca oil sands of Northern Alberta.

Figure 4 Crosswell survey geometry (schematic).

Figure 5: Ray density map (direct arrival, straight rays).

Figure 6: Common receiver gather, receiver depth: 205 m.

Figure 7: The configuration of the available wells relative to the source and receiver wells (wells 8 and 9, respectively).

Figure 8: The velocity tomogram. The velocity dispersion observed at the well bore results from the difference between sonic and crosswell seismic frequencies.

Figure 9: The attenuation tomogram.

Figure 10: *Q* tomogram. The distinct red zone near the top of the tomogram (depth interval 178 m – 188 m) is the related to the cap rock shale.

Figure 11: Viscosity tomogram generated using the left (decreasing) side of the BISQ curves.

Figure 12: Viscosity tomogram generated using the right (increasing) side of the BISQ curves.

Parameter	Value	Unit
Fluid density	1,000	kg/m^3
Fluid bulk modulus	0.8	*GPa*
Fluid saturation	1	
Porosity	0.25	
Permeability	2,000	*md*
Characteristic length	1	*mm*
Matrix bulk modulus	35	*GPa*
Matrix density	2,650	kg/m^3
Frame bulk modulus	1.7	*GPa*
Frame shear modulus	1.35	*GPa*
Frequency	300	*Hz*

Table 1: Reservoir parameters used for generating the graph shown in Figure 1.

Parameter	Value
Bulk modulus (quartz)	$36.6\times10^{9}\ pa$
Shear modulus (quartz)	$45\times10^{9}\ pa$
Bulk modulus (clay)	$25\times10^{9}\ pa$
Shear modulus (clay)	$9\times10^{9}\ pa$
Bulk modulus (water)	$2.2\times10^{9}\ pa$
Shear modulus (water)	$0\ pa$
Bulk modulus (oil)	$3\times10^{9}\ pa$
Characteristic squirt flow length	$0.5\,mm$

Table 2: The values assumed for the reservoir rock and fluid properties.

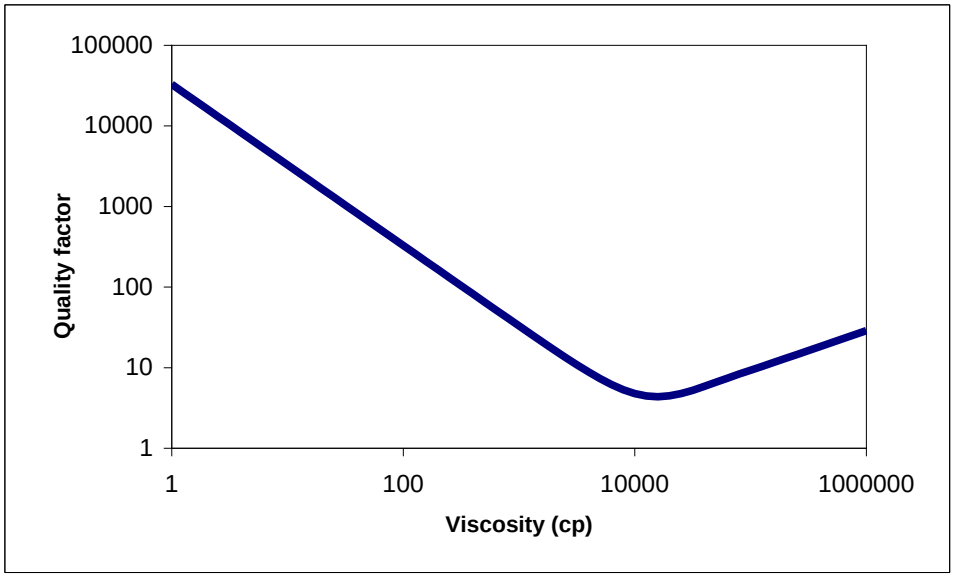

Fig. 1. Variation of quality factor with fluid viscosity predicted by BISQ theory. Reservoir parameters are given in Table 1.

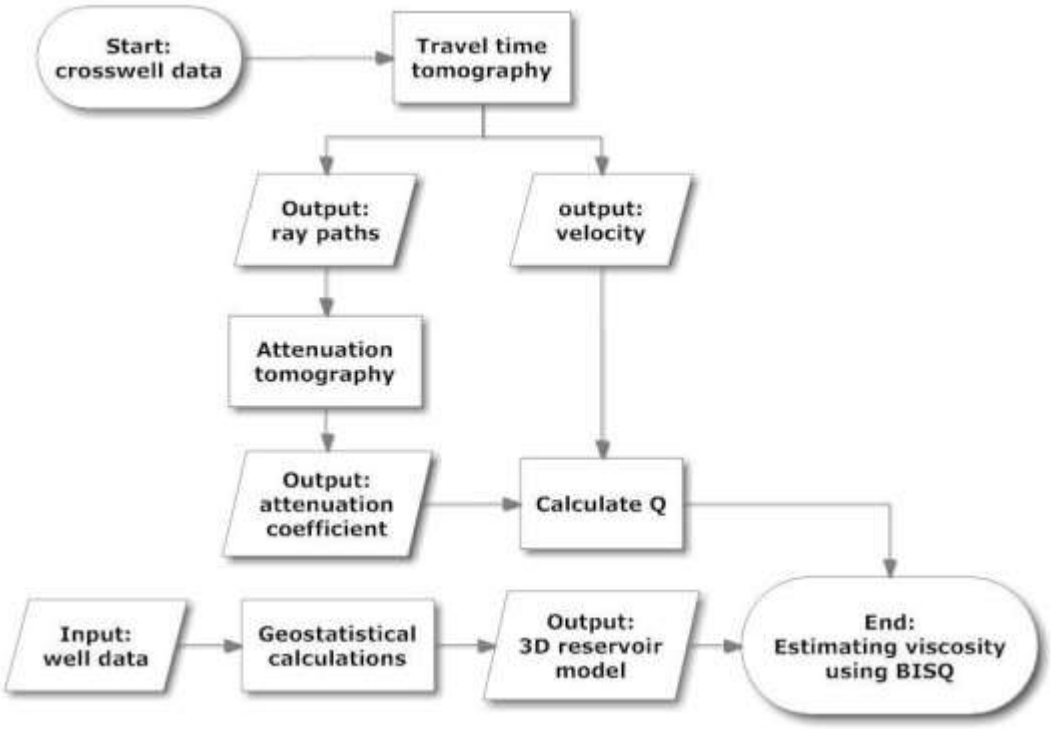

Fig. 2. Workflow for estimating viscosity from crosswell seismic data.

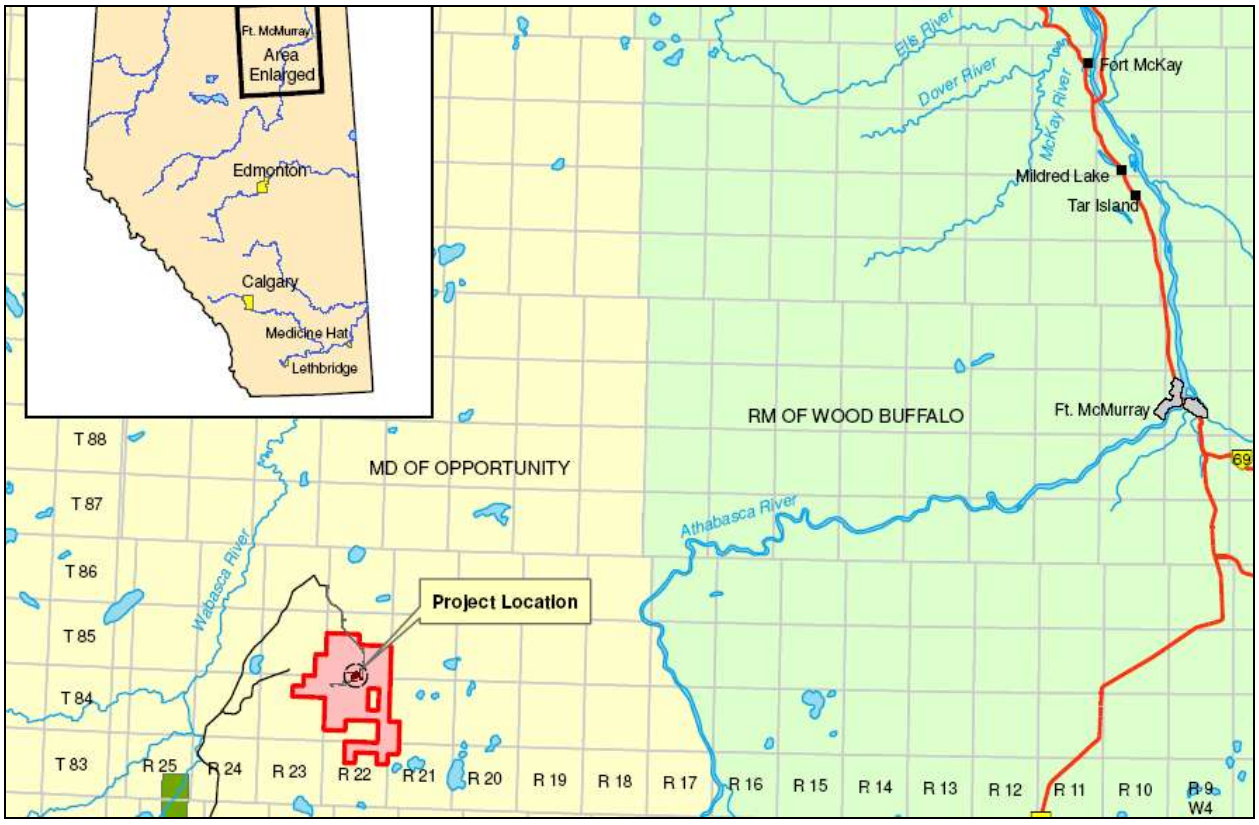

Fig. 3. Location of the crosswell survey in the Athabasca oil sands of Northern Alberta.

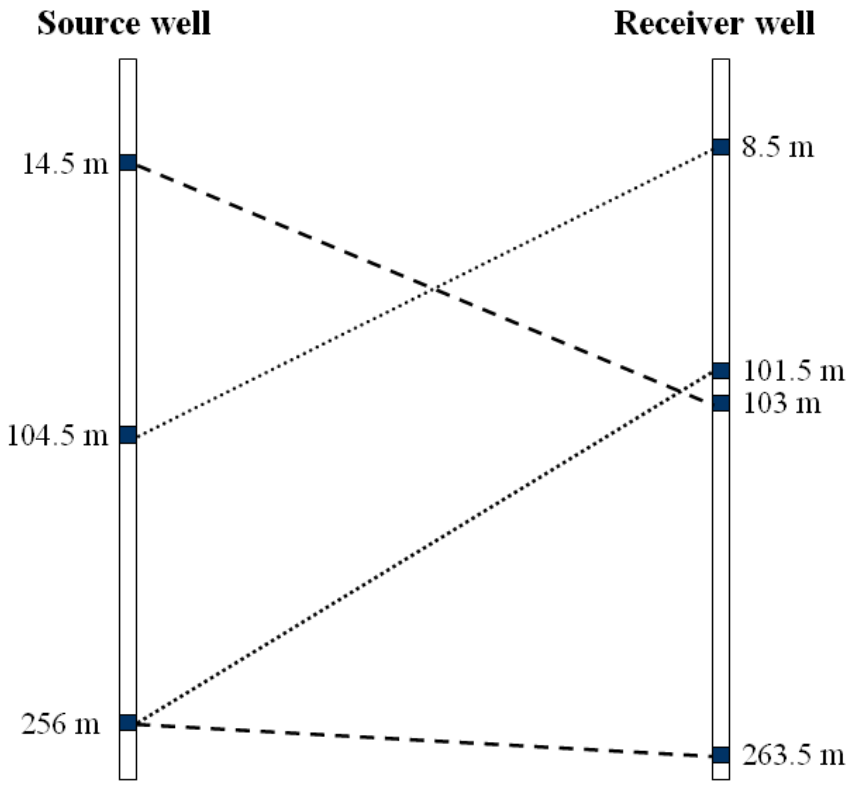

Fig. 4. Crosswell survey geometry (schematic).

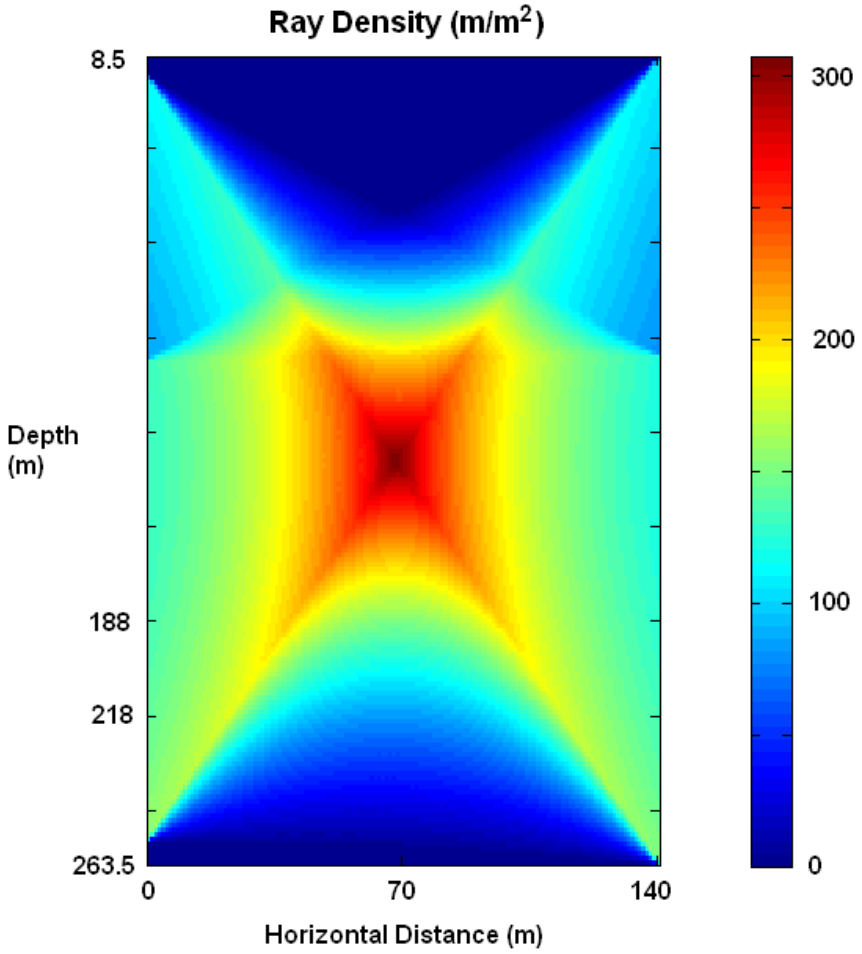

Fig. 5. Ray density map (direct arrival, straight rays).

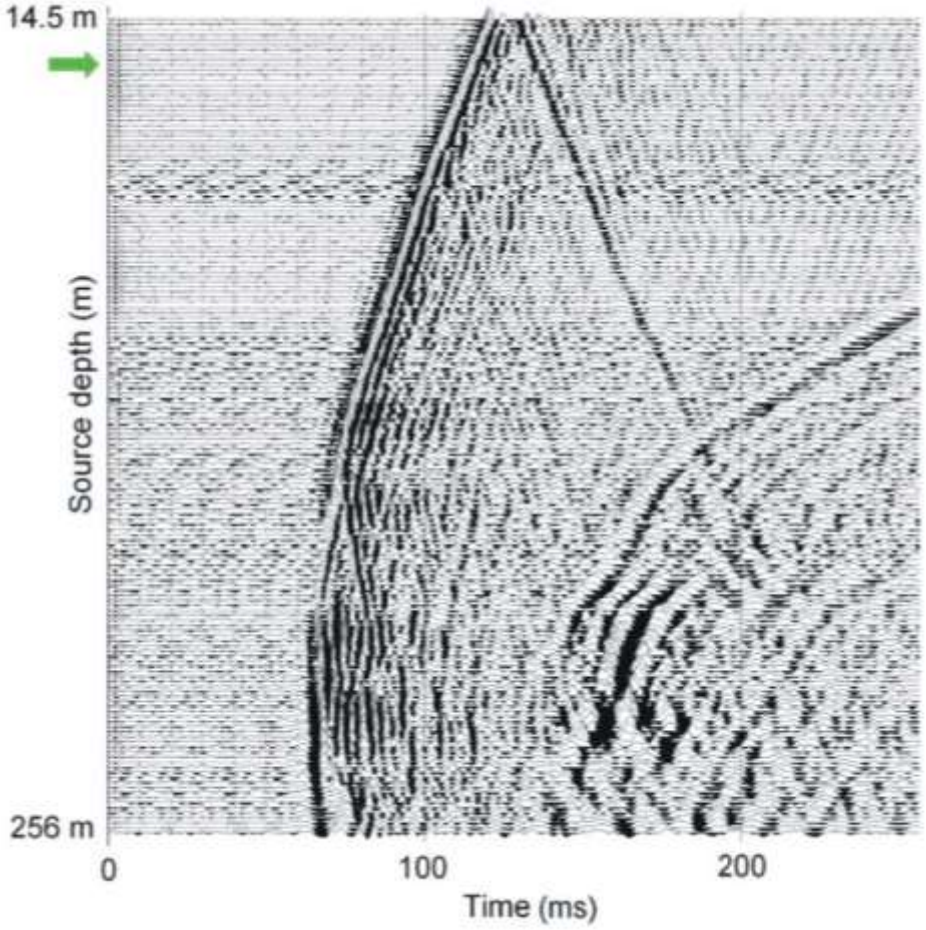

Fig. 6. Common receiver gather, receiver depth: 205 m.

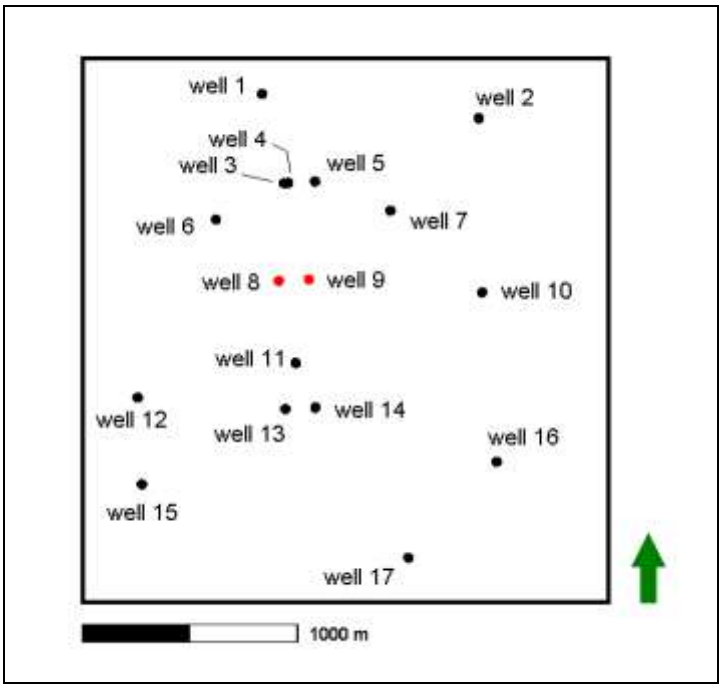

Fig. 7. The configuration of the available wells relative to the source and receiver wells (wells 8 and 9, respectively).

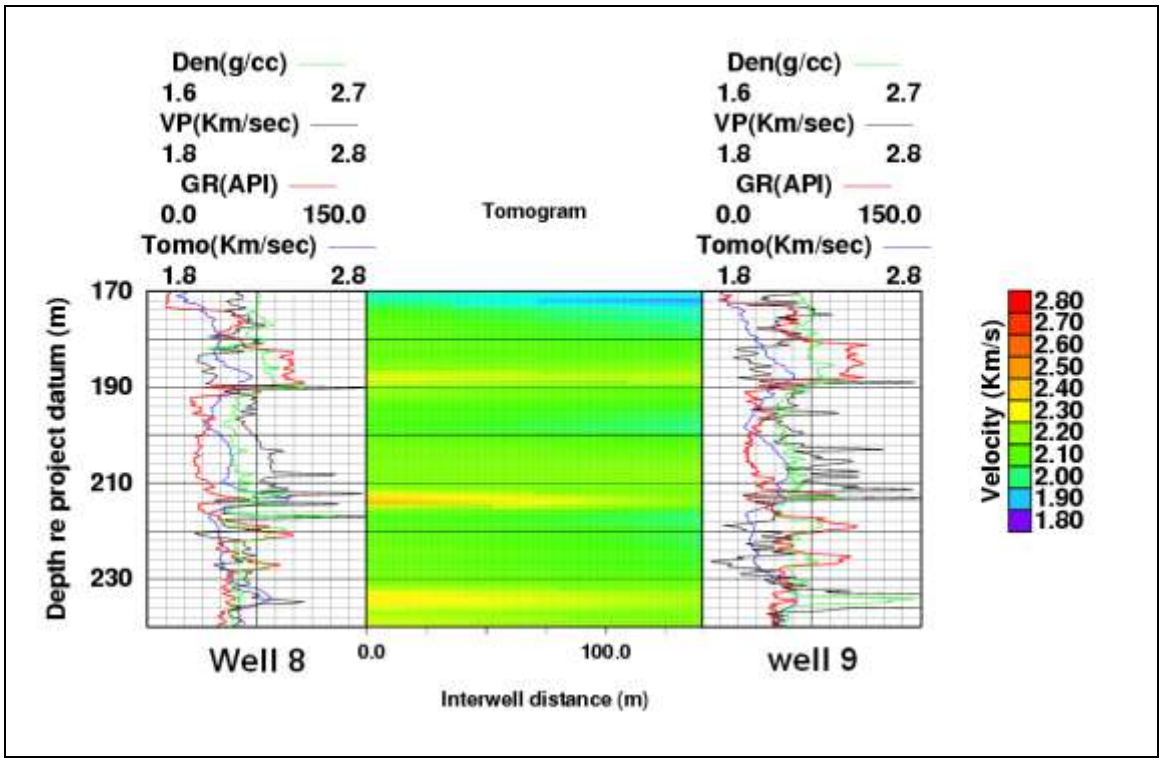

Fig. 8 The velocity tomogram.

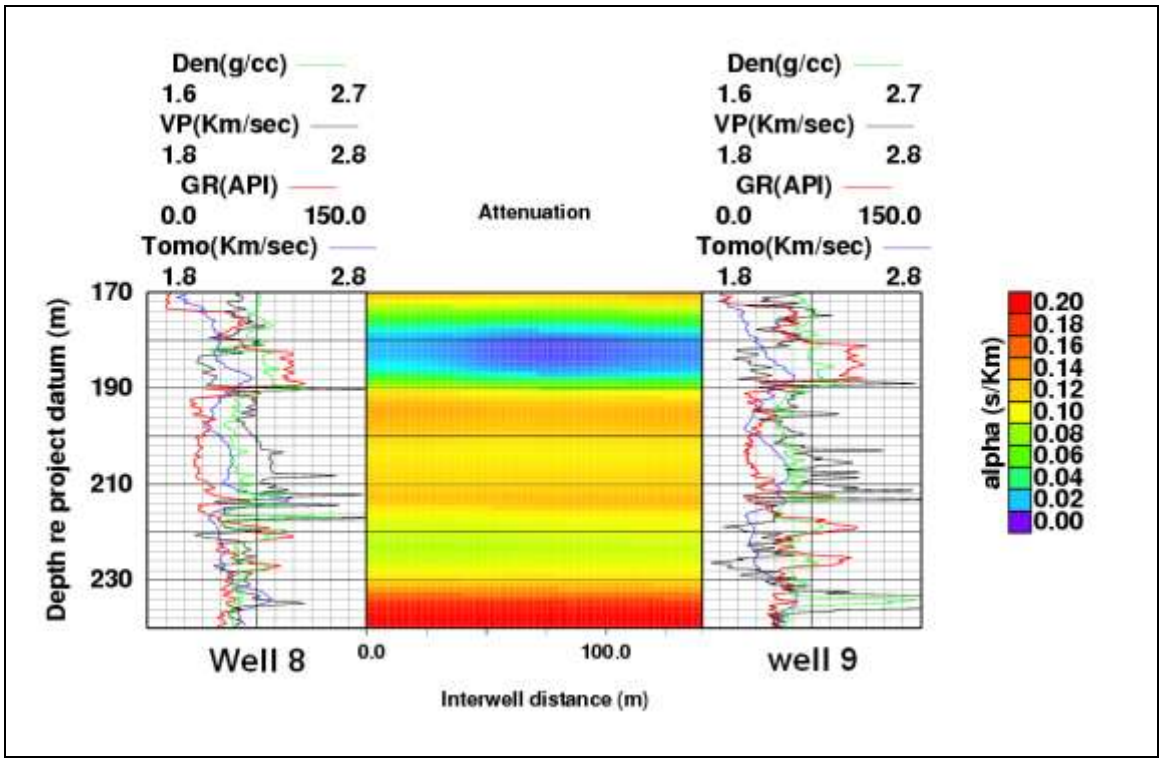

Fig. 9. The attenuation tomogram.

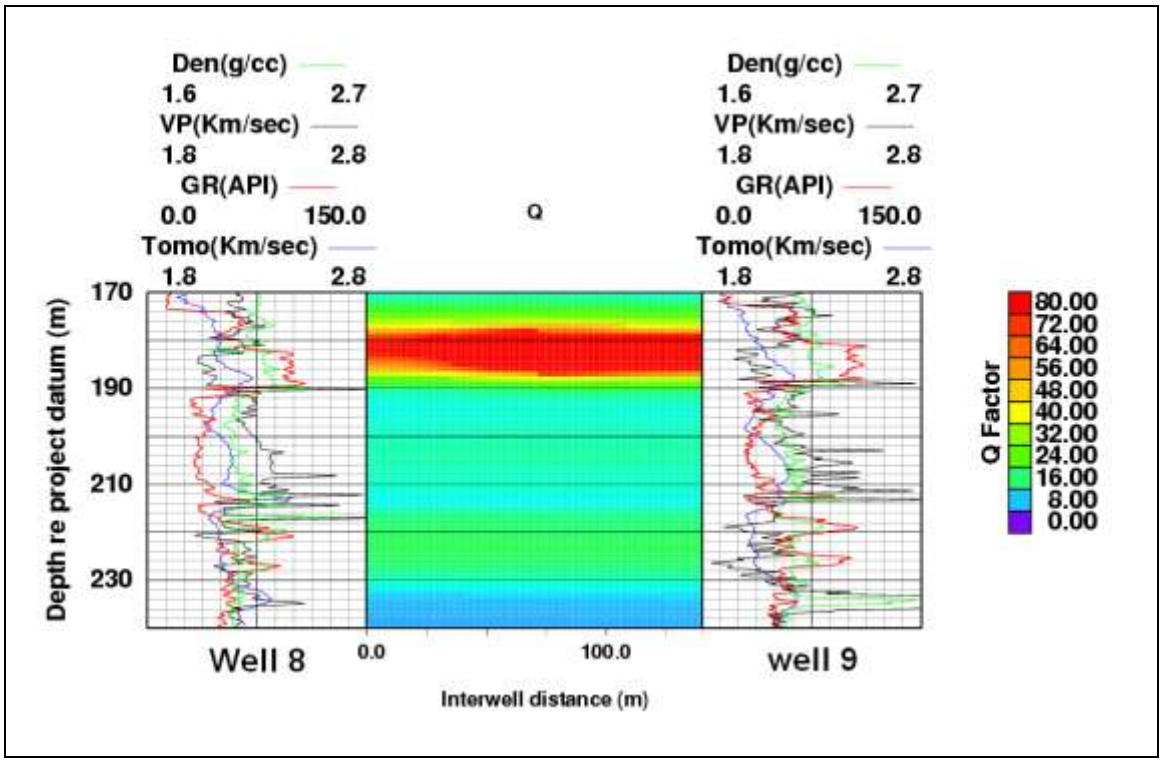

Fig. 10. The *Q* tomogram.

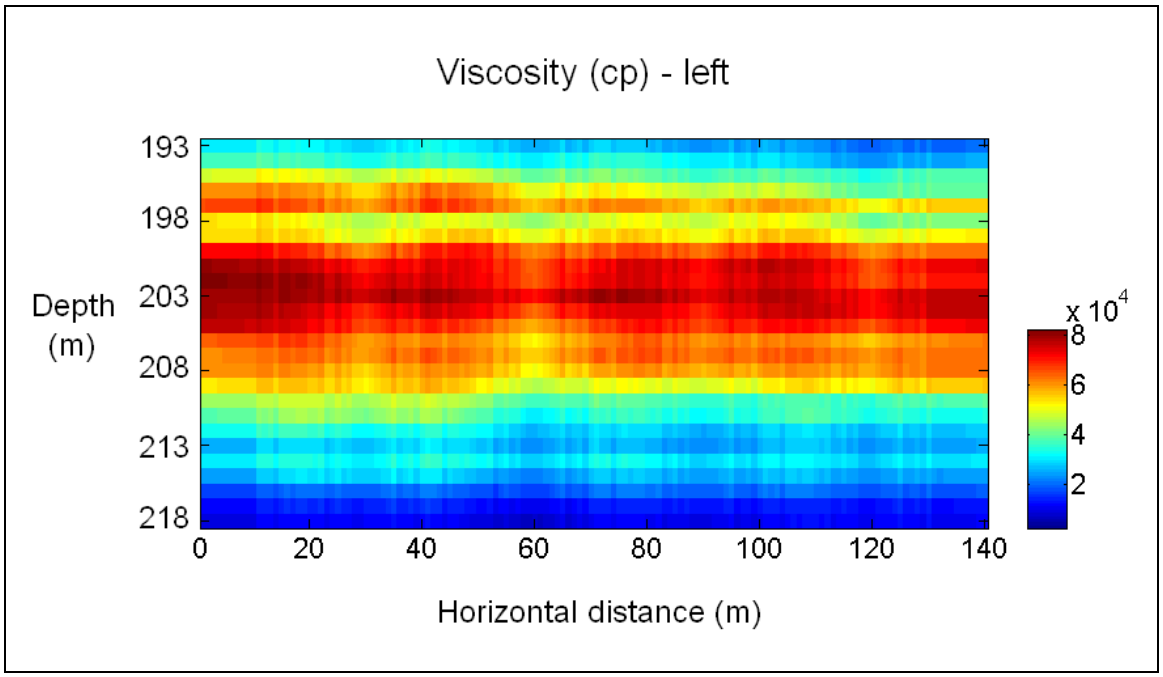

Fig. 11. Viscosity tomogram generated using the left (decreasing) side of the BISQ curves.

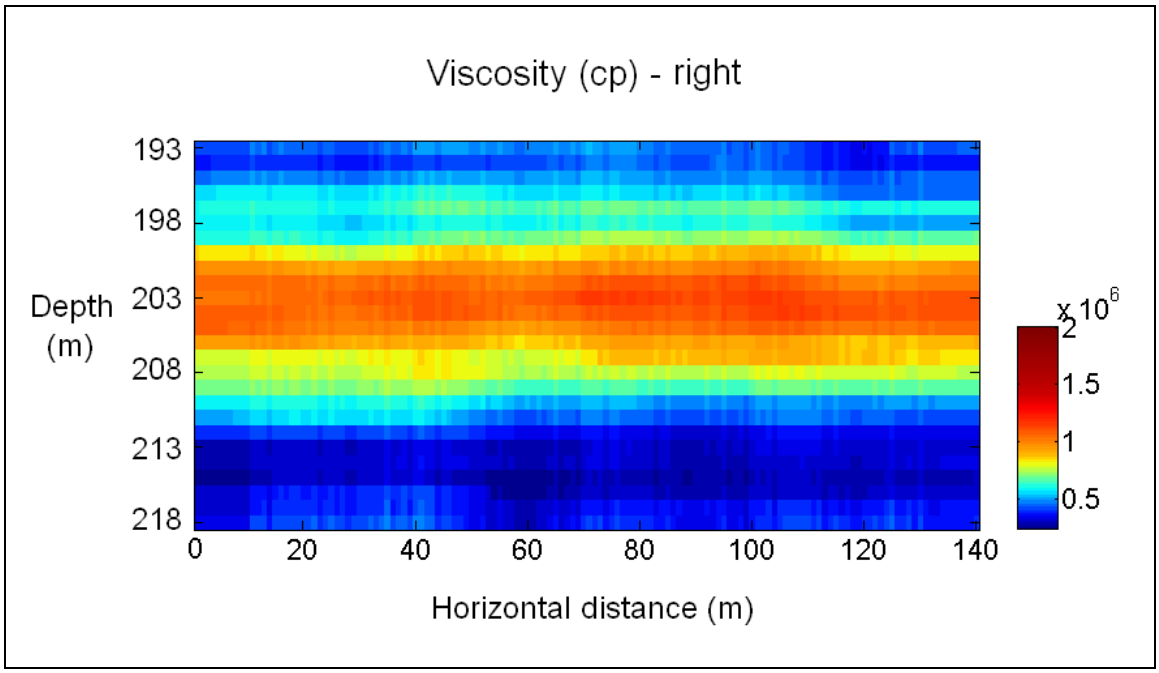

Fig. 12. Viscosity tomogram generated using the right (increasing) side of the BISQ curves.